Ultra Low Frequency Waves at the Ground Driven by the Kelvin-Helmholtz Instability Associated with Reconnection: A Case Study

Jamie Gorman[1,2,3], Elena A. Kronberg[2], Katariina Nykyri[4], Artem Smirnov[5,2,6], Jesper W. Gjerloev[7,8], Elena E. Grigorenko[9,10], Liudmyla V. Kozak[11,12], Karlheinz J. Trattner[13], and Matthew Friel[8]

[1]Max Planck Institute for Solar System Research, Göttingen, Germany.
[2]Department of Earth and Environmental Sciences, Ludwig-Maximilians University of Munich, Munich, Germany.
[3]Technical University of Munich, Munich, Germany.
[4]Center for Space and Atmospheric Research, Physical Sciences Department, Embry-Riddle Aeronautical University, Daytona Beach, Florida, USA.
[5]Helmholtz-Centre Potsdam - GFZ German Research Centre for Geosciences, Potsdam, Germany
[6]Geophysical Center of the Russian Academy of Sciences, Moscow, Russia.
[7]Department of Physics and Technology, University of Bergen, Bergen, Norway.
[8]The Johns Hopkins University Applied Physics Laboratory, Laurel, Maryland, USA.
[9]Space Research Institute, Russian Academy of Sciences, Russia.
[10]Moscow Institute of Physics and Technology, Moscow, Russia.
[11]Taras Shevchenko National University of Kyiv, Kyiv, Ukraine.
[12]Space Research Institute of the National Academy of Sciences of Ukraine and State Space Agency of Ukraine, Kyiv, Ukraine.
[13]Laboratory for Atmospheric and Space Physics, Boulder, Colorado, USA.

Key Points:

- Kelvin-Helmholtz (KH) waves at the magnetopause were observed by Cluster during southward IMF.
- ULF waves were recorded at the same time by ground-based geomagnetic observatories.
- ULF wave characteristics were consistent with the KH waves as the driver.

Corresponding author: Elena A. Kronberg, kronberg@geophysik.uni-muenchen.de

Abstract

The Kelvin-Helmholtz instability (KHI) and its effects relating to the transfer of energy and mass from the solar wind into the magnetosphere remain an important focus of magnetospheric physics. One such effect is the generation of Pc4-Pc5 ultra low frequency (ULF) waves (periods of 45-600 s). On 3 July 2007 at $\sim$ 0500 magnetic local time (MLT) the Cluster space mission encountered Pc4 frequency Kelvin-Helmholtz waves (KHWs) at the magnetopause with signatures of persistent vortices. Such signatures included bipolar fluctuations of the magnetic field normal component associated with a total pressure increase and rapid change in density at the vortex edges, oscillations of magnetosheath and magnetospheric plasma populations, wave frequencies within the expected range of the fastest growing KH mode, and magnetopause conditions favorable to the onset of the KHI. The event occurred during a period of southward polarity of the interplanetary magnetic field. Most of the KHI vortices were associated with reconnection indicated by the Walén relation, the presence of deHoffman-Teller frames and field-aligned ion beams. Global magnetohydrodynamic (MHD) simulation of the event also resulted in KHWs at the magnetopause. The observed KHWs associated with reconnection coincided with recorded ULF waves at the ground whose properties suggest that they were driven by the KHWs. Such properties were the location of Cluster's magnetic foot point, the Pc4 frequency, and the solar wind conditions.

Plain Language Summary

The Earth's magnetosphere acts as a protective barrier between our planet and the charged particles streaming out from the sun, the solar wind. When the solar wind is able to breach this barrier, there can be adverse consequences for the satellite, power, and electrical systems relied upon by humans. Thus, it is important to understand the various ways in which the solar wind particles and energy can be transferred into the inner magnetosphere. One way in which this occurs is through the Kelvin-Helmholtz instability. Waves can develop at the boundary between the faster moving solar wind and the slower moving magnetospheric plasma. It has been proposed that the energy from these waves can lead to strong disturbances in the magnetic field recorded on Earth. This study focuses on one event where Kelvin-Helmholtz waves observed by spacecraft in the magnetosphere induced such disturbances recorded at ground-based magnetic field observatories.

1 Introduction

The Kelvin-Helmholtz instability (KHI) at the magnetopause has been noted for its role in the transport of mass and energy from the solar wind into the magnetosphere [e.g., *Fairfield et al.*, 2000; *Otto and Fairfield*, 2000; *Nykyri and Otto*, 2001; *Hasegawa et al.*, 2004]. The KHI has been found to occur fairly frequently under both southward and northward interplanetary magnetic field (IMF) configurations with no apparent low-speed cutoff [*Kavosi and Raeder*, 2015; *Yu and Ridley*, 2013]. When the IMF horizontal component is mostly in the Parker-Spiral (PS) orientation, the KHI has been shown to favor the dawn flank magnetopause [*Henry et al.*, 2017]. This possible explains the dawn-dusk asymmetry of the Pc4-Pc5 range ultra low frequency (ULF) waves [*Nykyri and Dimmock*, 2016] and enhanced heating of the cold-component ions at the dawn sector [*Wing et al.*, 2005; *Moore et al.*, 2017] as the horizontal component of the IMF is most often in the PS orientation [*Dimmock and Nykyri*, 2013]. One proposed manner in which energy transfer is achieved by the KHI is through the generation of ULF waves. ULF waves have been shown to drive auroral arcs through magnetic field line resonance (FLR) [*Lotko et al.*, 1998] and to efficiently accelerate energetic electrons in the outer radiation belt [*Elkington et al.*, 2003; *Kronberg et al.*, 2017].

Pc4-Pc5 band (frequencies of 2-22 mHz, periods of 47-600 s) ULF waves are believed to be generated by KHIs through a coupling between the magnetopause surface waves and resonant field lines, as shown in theoretical work by e.g., *Southwood* [1974] and in statistical study by *Nykyri and Dimmock* [2016]. Since ULF waves can be detected by ground-based magnetic observatories, it is possible to correlate these observations with satellite observations of the KHI. However, debate remains regarding whether or not the KHI is an actual, dominant driver for Pc4-Pc5 pulsations [*Hasegawa*, 2012], especially under southward IMF conditions when other possible external drivers, such as flux transfer events, occur and interact with the KHI [*Bentley et al.*, 2018].

The proposal that the KHI drives ULF waves is not a new one. *Hasegawa and Chen* [1974] and *Southwood* [1974] showed theoretically that magnetic field line resonance oscillations can be caused by Kelvin-Helmholtz waves (KHWs) at the magnetopause. More recently, *Rae et al.* [2005] investigated ULF pulsations at the magnetopause (believed

to be KHWs but without explicit evidence) which were observed to propagate into the magnetosphere and down into the ionosphere in the dusk sector under fast solar wind speeds. Similarly, *Agapitov et al.* [2009] presented THEMIS magnetic field observations at the dawn flank of magnetopause oscillations that coincided with ULF pulsations recorded deeper in the magnetosphere. The magnetopause surface waves were hypothesized to be KHWs based upon the critical velocity for KHI onset and wave growth [*Walker*, 1981]. *Dougal et al.* [2013] modeled several instances of the KHI observed at the magnetospheric flanks under northward IMF to gain better insight into the resulting ionospheric signatures. Pc5 magnetic field oscillations within the ionospheric foot point ranges of some of these events were observed. *Wang et al.* [2017] investigated magnetospheric Pc5 pulsations under steady solar wind conditions and made the case that ULF waves can not only be driven by FLR or waveguide modes [*Hasegawa and Chen*, 1974], but also through the generation of inner and outer Kelvin-Helmholtz modes.

Since other processes can externally drive ULF waves in the magnetosphere, it has been argued that it is likely these mechanisms that are the true drivers, occurring in conjunction with the KHI at the magnetopause. Such processes relate to high solar wind speeds and include dynamic pressure variations and foreshock fluctuation anisotropy instabilities [*Hasegawa*, 2012].

One of the greater difficulties involved in settling this current debate is the lack of appropriate empirical data. This is due to the spatial and temporal limitations associated with satellite data collection. However, with the increase of satellite missions within the past few decades, more opportunities for data analysis have arisen. In particular, ESA's Cluster space mission has the advantage of providing multi-point observations. Presented herein is a Cluster-observed incidence of KHI-driven ULF waves under conditions that refute the above counterarguments. This event adds to the few previously published KHW-ULF linked events [*Rae et al.*, 2005; *Agapitov et al.*, 2009; *Dougal et al.*, 2013], but provides an even more comprehensive analysis of the magnetopause surface waves, investigating the magnetic field data in conjunction with plasma particle observations for KHI signatures. Furthermore, as the present event occurs for the southward IMF orientation, both magnetic reconnection and KHI can start as a primary mode [*Ma et al.*, 2014a,b]. For southward IMF conditions, fast magnetic reconnection is driven and can be strongly modified by the nonlinear KH waves: MHD and Hall-MHD simulations have indicated that reconnection rates are comparable to Petschek reconnection even without the in-

clusion of Hall physics [*Ma et al.*, 2014a]. On the other hand, magnetic reconnection can seed the KH mode for KH unstable conditions [*Ma et al.*, 2014b]. KHI vortices in our event are associated with reconnection signatures, making the case more comprehensive.

The observed magnetospheric conditions were also modeled to further test if the magnetic field configuration was KHI-unstable. Finally, the satellite observed KHWs were compared with concurrent ULF pulsations measured at ground, allowing for the connection between magnetic disturbances seen in space and those seen on Earth.

2 Spacecraft Observations

On 3 July 2007 from 1645-1720 UT, the Cluster spacecraft approached the border between the magnetosheath and the dawn side magnetopause (the coordinates in Geocentric Solar Ecliptic (GSE) system were X ≈ -10 R_E, Y ≈ -15 R_E, Z ≈ -9.4 R_E). Observed plasma signatures of this event are shown in Figure 1. These measurements, which were obtained through the Cluster Science Archive (CSA) [*Laakso et al.*, 2010], came from the Cluster Ion Spectrometry (CIS) experiment's [*Rème et al.*, 2001] COmposition and DIstribution Function (CODIF) sensor and the Hot Ion Analyser (HIA). Further documentation regarding the Cluster mission can be found through *Escoubet et al.* [1997].

The ion density and velocity profiles measured by the CIS/HIA instrument, in conjunction with the proton (H+) and ion energy spectrograms measured by the CIS/CODIF and CIS/HIA instruments, showed the oscillation of plasma populations (see Figure 1). Bipolar velocity fluctuations from the strongly anti-sunward to the weakly anti-sunward or sunward direction were experienced by both Cluster spacecraft (SC) 1 and 3 starting after 16:45 UT (HIA data were unavailable for SC 2 and 4 during the event). The proton energy spectrogram for SC 4 and the ion energy spectrogram for SC 1 displayed similar alternations between high-energy (∼10 keV) plasma and lower energy (∼1 keV) plasma. Those alternations corresponded with fluctuations in the SC 1 and 3 ion densities from tenuous (< 1 cm^{-3}) to dense (3-10 cm^{-3}), respectively. These fluctuations indicate that the spacecraft were observing alternating regimes between the magnetosheath and the magnetosphere.

The OMNI-calculated solar wind parameters during this event can be found in Figure 2. There was a solar wind speed of 375 km s^{-1} and the B_Z component of the IMF

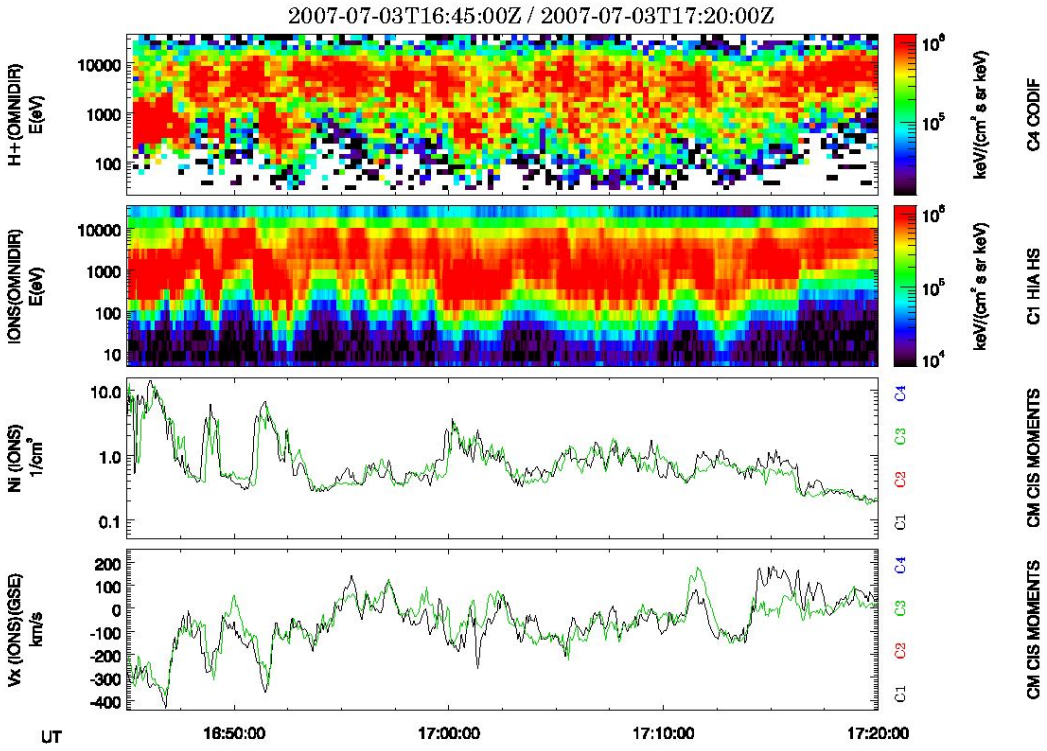

Figure 1. Cluster CIS observations from 3 July 2007, 16:45-17:20 UT. From top to bottom: CODIF energy-time spectrogram of proton differential energy flux, keV/(cm^2 s sr keV), from SC 4; HIA ion differential energy flux, keV/(cm^2 s sr keV), from SC 1; ion density, cm^{-3}, from SC 1 & 3; X-component ion velocity, km s^{-1} (GSE), from SC 1 & 3.

was southward. The horizontal component of the IMF was in Parker spiral orientation ($B_X \approx 5$ nT, $B_Y \approx$ -6 nT). There were pressure fluctuations up until about 16:35 which then ceased and remained rather stable throughout the event time frame. The Dst index (not shown) revealed that there wasn't a geomagnetic storm during the time of the event, however the AE index indicated that a geomagnetic substorm had occurred.

The proton density, total pressure including its magnetic and plasma components, velocity and magnetic field profiles for the first half of the event using Cluster SC 4 data are shown in Figure 3. The observed magnetic field components were measured by Cluster's onboard fluxgate magnetometer (FGM) [*Balogh et al.*, 2001]. The magnetic field and velocity data for the time interval from 16:40 to 17:45 UT were transformed to the (L, M, N) components using the minimization of the Faraday residue (MFR) technique as detailed by e.g., *Khrabrov and Sonnerup* [1998]. The coordinate vectors L and M are

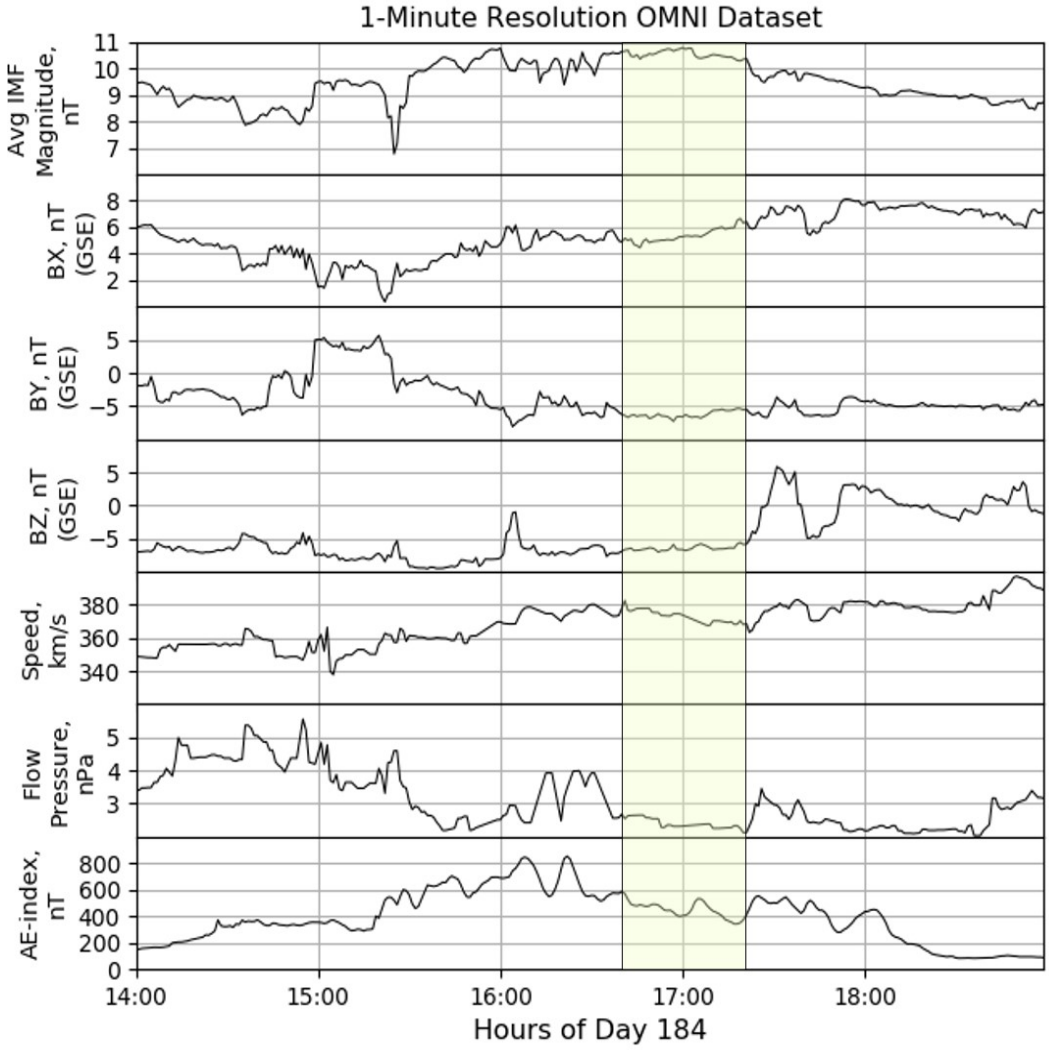

159 **Figure 2.** OMNI derived solar wind parameters for 3 July 2007 from 1400-1900 UT. The
160 highlighted portion represents the time frame of the observed KHI from 16:40-17:20. From top to
161 bottom: average IMF magnitude, nT; B_X, nT; B_Y, nT; B_Z, nT; speed, km/s; flow pressure, nPa;
162 and AE index, nT.

186 mutually orthogonal and tangential to the boundary. L = [-0.17, -0.96, 0.22] and is di-
187 rected mostly dawnward along the Geocentric Solar Magnetospheric (GSM) Y axis. M
188 = [-0.81, 0.26, 0.52] and is directed mostly antisunward along XGSM. N is the coordi-
189 nate vector in the boundary normal direction. It is orthogonal to L and M, forming a
190 right-handed coordinate system. N = [-0.56, -0.10,-0.82] and is directed mostly south-
191 ward along the ZGSM axis. The eigenvaluesof the system are $[\lambda_1, \lambda_2, \lambda_3]$ = [4.35, 3.68,
192 0.94]. The ratio λ_2/λ_3=3.92, indicating that the normal direction is well defined. The

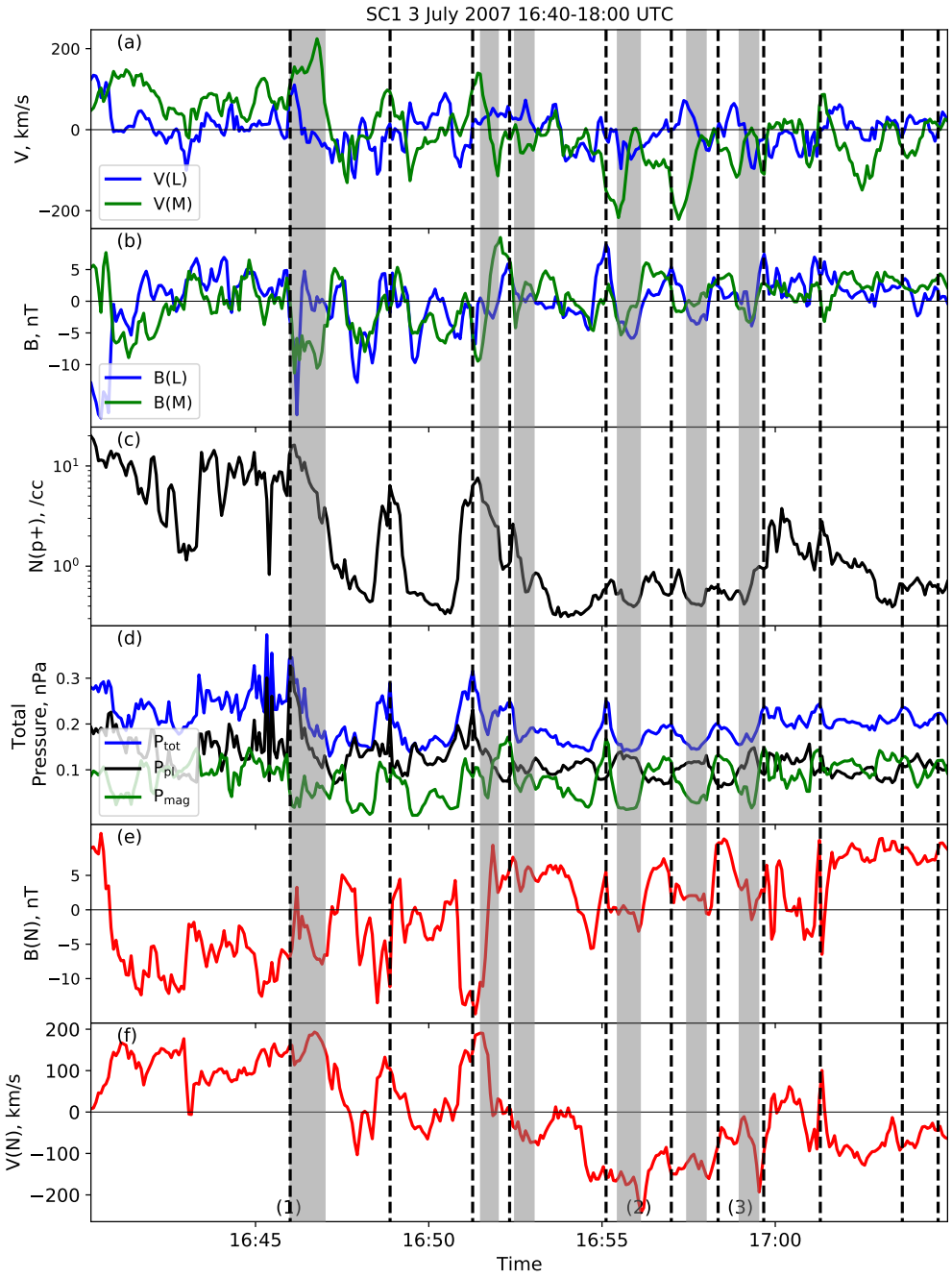

Figure 3. SC 4 measured and derived parameter profiles for the KHI event on 3 July 2007 are shown for the time frame of 1640–1705 UT. From top to bottom within each graph: (a) transformed velocity components L (blue) and M (green), km s^{-1}; (b) transformed magnetic components L (blue) and M (green), nT; (c) proton density (black), cm^{-3}; (d) total/plasma/magnetic pressure (blue/black/green), nPa; (e) transformed magnetic normal component (red), nT; (f) transformed velocity normal component (red), km s^{-1}. The vertical black dashed lines indicate the times of strong maxima in the total pressure profile. The vertical shadowed bars show location of rotational discontinuities. (1), (2) and (3) indicate time intervals for which field-aligned beams were observed (see Figure 5).

vectors L and M are interchangeable because $\lambda_1 \simeq \lambda_2$. A suitably well-defined MFR normal direction was also found for SC 1 during the event (not shown). The total pressure was calculated as the sum of the magnetic (p_{mag}) and plasma pressures (p), both shown in Figure 3, such that:

$$p_{mag} = \frac{B^2}{2\mu_0} \tag{1}$$

$$p = nk_BT \tag{2}$$

with B = magnetic field strength, μ_0 = permeability of free space, n = plasma (proton) density, k_B = Boltzmann's constant, and

$$T = \frac{2T_\perp + T_\parallel}{3} \tag{3}$$

where $T_\perp$ = plasma proton perpendicular temperature and $T_\parallel$ = proton parallel temperature. The plasma proton temperature measurements were taken from the CIS/CODIF instrument.

Bipolar fluctuations in the normal component of the magnetic field occurred throughout the entirety of the event, from 1645 to 1705 UT (see Figure 3). The proton density, total pressure, velocity and other magnetic component profiles were also highly oscillatory. The vertical dashed lines mark the local total pressure maxima which are mostly aligned with the local absolute maxima of B_N, not the bipolar crossings at B_N=0, which is a signature of a hyperbolic point of the rolled-up KHWs [*Hasegawa et al.*, 2004; *Hasegawa*, 2012] (see Discussion below). The jumps in the density are mostly associated with maxima of the total pressure.

KH waves are unstable if

$$\left(\vec{k}\cdot(\vec{V}_{\rm msh}-\vec{V}_{\rm msp})\right)^2 > \left((\vec{k}\cdot\vec{B}_{\rm msh})^2+(\vec{k}\cdot\vec{B}_{\rm msp})^2\right)/4\pi\rho^*,$$

where $\rho^* = \rho_{\rm msh}\rho_{\rm msp}/(\rho_{\rm msh}+\rho_{\rm msp})$ is the mean mass density, $\vec{k}$ is the wave vector, V is the plasma velocity, B is the magnetic field and msh/msp is magnetosheath/magnetosphere [*Johnson et al.*, 2014]. From the observations we consider the time period at 16:48 UT. We took $\vec{k}$=$\vec{M}$, where M is the direction along the magnetopause for data transformed in MFR coordinates and the following values of $\rho_{\rm msp}$=0.5 cm^{-3}, $\rho_{\rm msh}$=6 cm^{-3}, $V_{\rm M\ msp}$=110 km s^{-1}, $V_{\rm M\ msh}$=100 km s^{-1}, $B_{\rm M\ msp}$=5·10^{-9} nT and $B_{\rm M\ msh}$=-4·10^{-9} nT. This will give

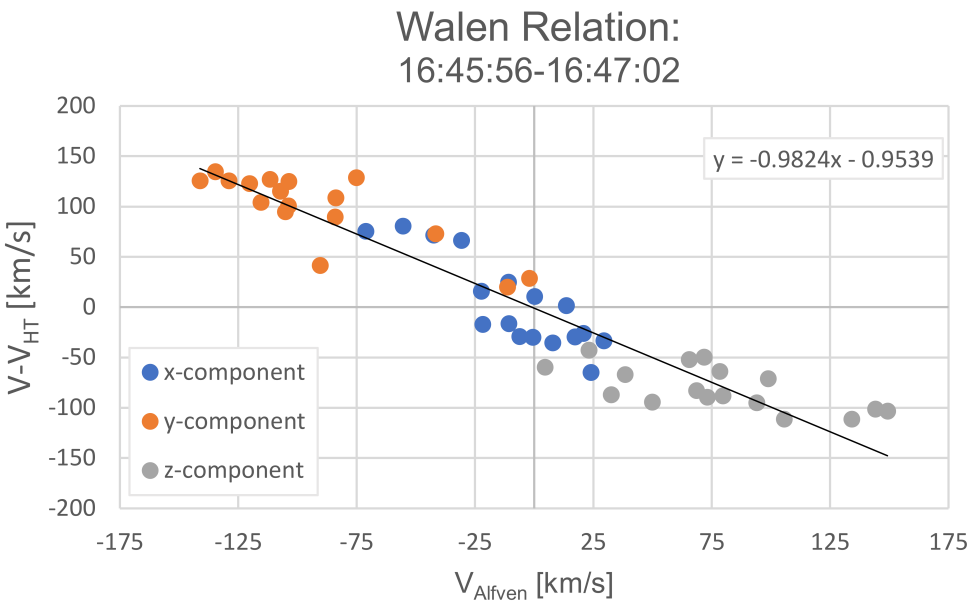

Figure 4. Walén relation calculated for the SC 4 observations during time interval 16:45:56-16:47:02 UT.

$\left(V_{\mathrm{M\ msh}} - V_{\mathrm{M\ msp}}\right)^2 = 4.4 \cdot 10^{11}$ km^2 s^{-2} $> \left(B^2_{\mathrm{M\ msh}} + B^2_{\mathrm{M\ msp}}\right)/4\pi\rho^* = 4.2 \cdot 10^{11}$ km^2 s^{-2}, implying that the environment observed by Cluster is unstable for KHI.

We also test if reconnection is observed during this event. For this we transform the velocity, $\vec{V_{HT}}$, into deHoffmann-Teller (HT) frame which is co-moving together with the discontinuity [*Sonnerup et al.*, 1995]. The HT velocity is determined by minimizing $|(\vec{V_{HT}} - \vec{V}| \times \vec{B}|^2$ to obtain the constant transformational velocity $\vec{V_{HT}}$ for a given dataset. Here $\vec{V}$ and $\vec{B}$ are the observed time series of the ion velocities and of the magnetic field. The Walén relation calculated in HT frame shows the relation between the plasma velocity in HT frame and the Alfvén velocity, $\vec{V_A} = \vec{B}/\sqrt{\mu_0 \rho}$ [*Sonnerup et al.*, 1995]. We found a 1-minute deHoffmann-Teller interval from 16:46:00-16:47:00 UT (HT slope is 0.99 and correlation coefficient (CC) is 0.99) where the Walén relation is very well met, see Figure 4. We calculated Walén slope = -0.98 and Walén CC = -0.95. The Walén slope was negative, which means the spacecraft crossed the rotational discontinuity (RD) tailward of the X-line [*Paschmann et al.*, 2005]. The interval is marked by a gray shadowed bar in Figure 3.

There were several other frames that met the "strict" HT qualifications (HT Slope = 0.9-1.1 and CC >0.95) according to *Nykyri et al.* [2006], but none meet the "strict"

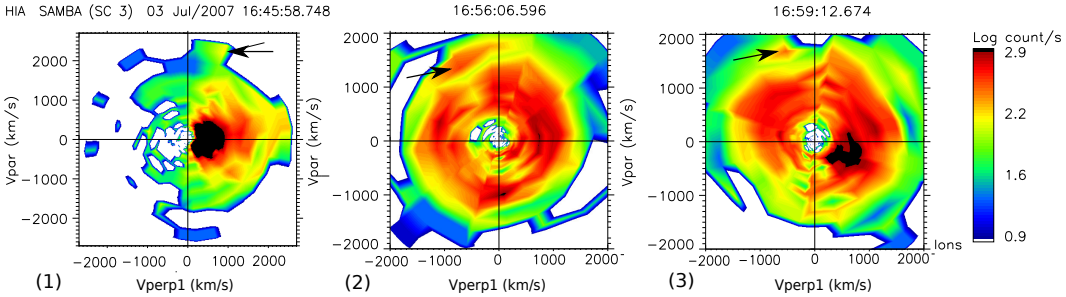

Figure 5. Ion velocity distribution functions in the parallel/perpendicular-plane as measured by the HIA instrument onboard SC3 at 16:45:58.748 UT (left), 16:56:06.596 UT (middle) and 16:59:12.674 UT (right). The black arrows indicate the field-aligned beams. The time of observation for distributions (1), (2), and (3) correspond to that similarity noted in Figure 3.

classification for an RD (HT Slope = 0.7-1.1 and CC >0.95). One, however, met a less-strict RD slope (>0.5). That was from 16:51:30-16:52:00 UT. If the correlation requirements and slope requirements for the Walén relation are both relaxed (CC>0.85, Walén slope>0.5), then four more RDs are seen at time intervals: 16:52:29 to 16:53:02 UT, 16:55:27 to 16:56:00 UT, 16:57:27 to 16:58:00 UT and 16:58:58 to 16:59:31 UT. All these intervals are marked by gray shadowed bars in Figure 3.

Field-aligned ion beams were observed at three instances during these intervals: 16:45:58.748 ($V_{\rm par}$=2300 km s^{-1}, $V_{\rm perp}$=900 km s^{-1}), 16:56:06.596 ($V_{\rm par}$=1400 km s^{-1}, $V_{\rm perp}$=-700 km s^{-1}) and 16:59:12.674 UT ($V_{\rm par}$=1700 km s^{-1}, $V_{\rm perp}$=-500 km s^{-1}), see Figure 5. This further indicates that reconnection had occurred.

In Figure 3 we can see that the hyperbolic points of the rolled-up KHWs indicated by the dashed lines are in most cases followed by rotational discontinuities likely associated with reconnection.

The spectral wavelet analysis of the magnetic field normal fluctuations as observed by Cluster is shown in Figure 6. The power peak in the global wavelet spectrum for the magnetic fluctuations is seen at a period of about 140 s. The period of 140 s approximately coincides with the frequency of the vertical lines (approximately every 112 s) drawn in Figure 3, namely with the reoccurrence frequency of KHI rolled-up vortex signatures. These are fluctuations within the Pc4 range.

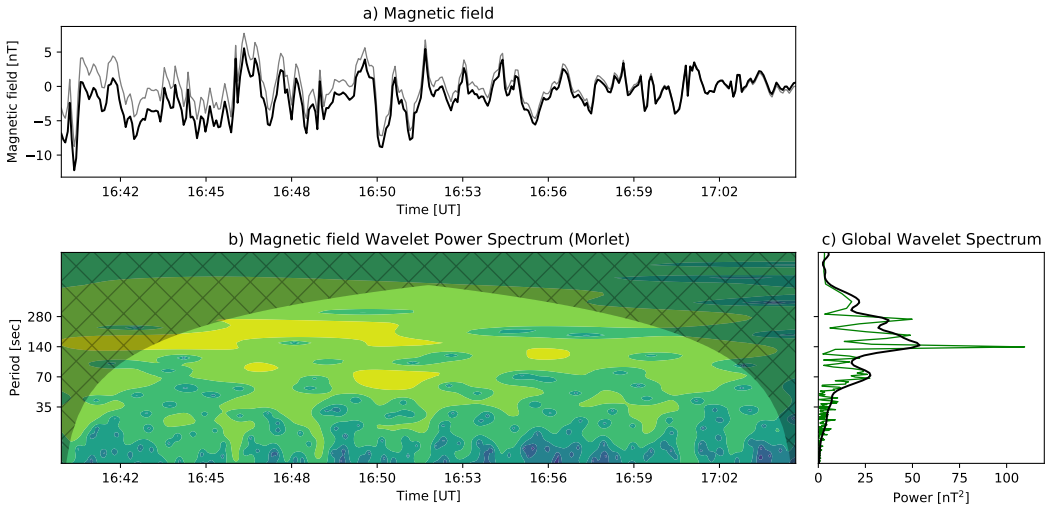

Figure 6. Wavelet transform analysis of MFR-derived magnetic field normal component, nT, from Cluster SC 4 between 16:40 and 17:05 UT: (a) original series (black) and inverse (gray) wavelet transform; (b) the normalized wavelet power spectrum and cone of influence hatched and (c) the global wavelet (black) and Fourier power spectra (green). Note that period scale is logarithmic.

3 Ground-based observations

During the same time period as the observed magnetopause fluctuations, large magnetic field disturbances were recorded at ground-based geomagnetic stations. These disturbances are shown in SuperMAG's Polar Plot (*Gjerloev* [2012]; see Figure 7). Also shown in Figure 7 is the estimated magnetic field line foot point from Cluster SC 4.

The magnetic foot point of the Cluster mission was mapped to the ionosphere by projecting the satellite location along the magnetic field lines to the altitude of 100 km, where the lower boundary of the ionosphere was assumed. Since the spacecraft was located at the magnetosheath boundary just outside the bounds of the magnetic field model, some adjustments were necessary in order to derive the magnetic foot point's location. In this case, the Z-coordinate of the spacecraft was assumed to be equal to -8.8 R_E instead of -9.4 R_E. Z = -8.8 R_E was the closest point to Z = -9.4 R_E where mapping was possible. The location of the magnetic foot point was derived using the Tsyganenko-1989 model of the external magnetic field (for K_p = 2.7), as implemented in the IRBEM library [*Boscher et al.*, 2012; *Shumko et al.*, 2018]. It is worth mentioning that magnetic

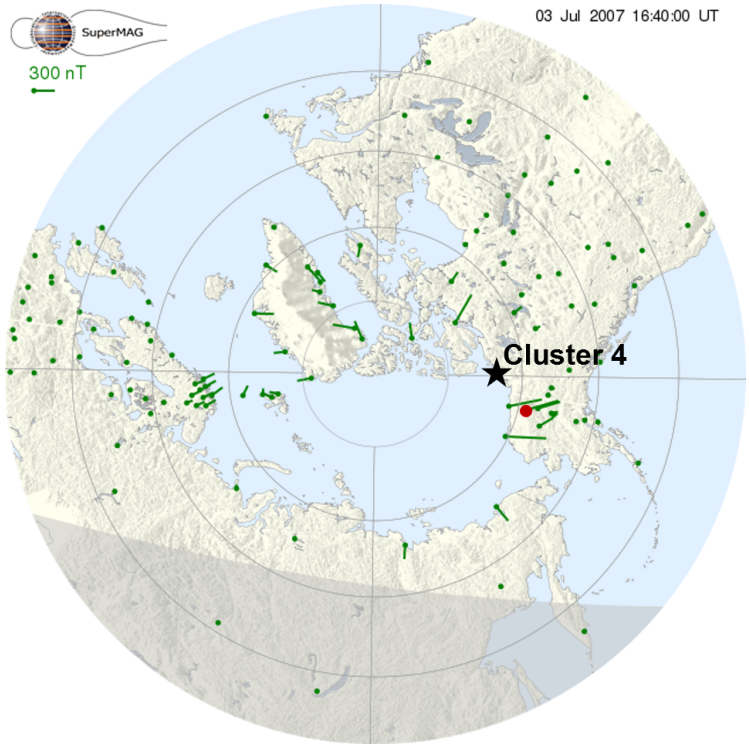

Figure 7. The SuperMAG Polar Plot is shown for 3 July 2007 at 16:40 UT. ULF waves at ground-based magnetometers are shown in red and the field line foot point corresponding to Cluster spacecraft 4 is shown. The green vectors represent the direction and magnitude of ground-based magnetic field disturbances. The approximate location of the Arctic Station (ARC) magnetometer is denoted by the red dot.

foot point tracing is highly model dependent (as shown in *Dunlop et al.* [2015]) and thus gives only an approximate indication of the spacecraft position with relation to the ionosphere.

The highest amplitude of ground-measured magnetic field disturbances in the SuperMAG Polar Plots were observed to be concentrated within the North Slope region of Alaska. While magnetic fluctuations were recorded at other geomagnetic variation stations around the polar cap, they were lower in amplitude and asymmetrically distributed. The magnetic field line foot point for Cluster SC 4 mapped to the NW coast of Canada, in the vicinity of the highest magnitude magnetic field fluctuations. These disturbances were possibly at least partially triggered by the flux transfer events (FTEs) in the northern hemisphere where they are likely to occur. Figure 8 shows the calculated magnetopause shear angle determined according to the event's specific solar wind parameters and ge-

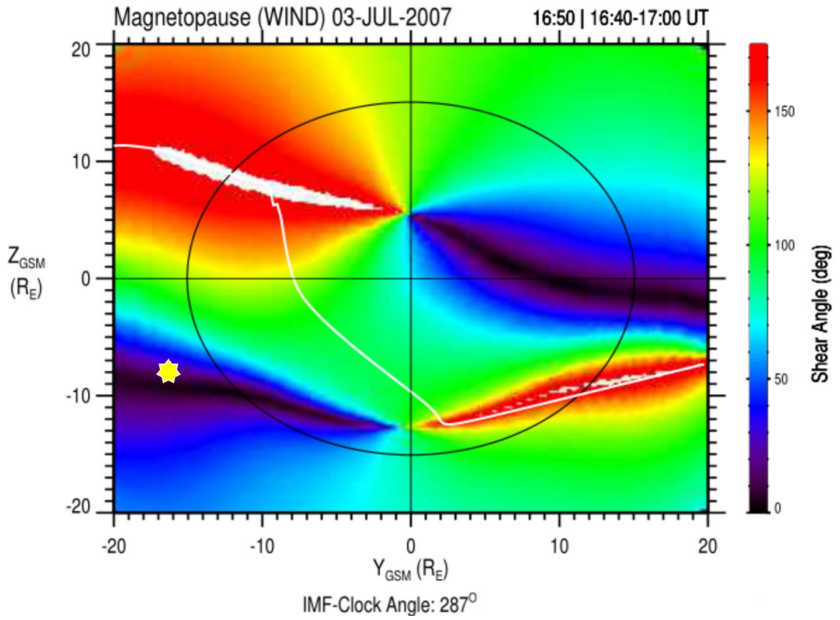

Figure 8. The magnetopause shear angle for IMF values $B_Z<0$, $B_Y<0$ as seen from the Sun. Red areas represent magnetopause regions where the geomagnetic field and IMF are antiparallel within 150°to 180°. White regions embedded in the red regions represent the line of maximum magnetic shear angles which are thought to be the most likely location for reconnection to occur. The black circle represents the location of the x=0 plane. Earth's dayside and nightside magnetopause are shown inside and outside of the black circle, respectively. The yellow star marks the location of Cluster spacecraft 4 ($X_{GSM}\approx$ -10 R_E, $Y_{GSM}\approx$ -16.2 R_E, $Z_{GSM}\approx$ -8 R_E).

omagnetic field (calculated from the T96 model). The white line depicts the maximum magnetic shear angle where magnetic reconnection had the highest probability of occurring [*Trattner et al.*, 2007, 2017], particularly at the dawn side of the northern hemisphere.

Our event showed magnetic field fluctuations at the magnetopause in the Pc4 frequency range. Therefore, to establish a link between the disturbances measured by Cluster in space and those recorded at ground-based magnetic field observatories, we needed to analyze those field measurements at a resolution of 1-10 s. The closest stations to the mapped Cluster location were Arctic Village (ARC) and Kaktovik, Alaska (KAV). The wavelet analysis for the magnetic field recorded at the magnetometer in ARC (as more clear) is shown in Figure 9. The analysis shows a wave power peak in the global wavelet spectrum for the E-component at 140 s.

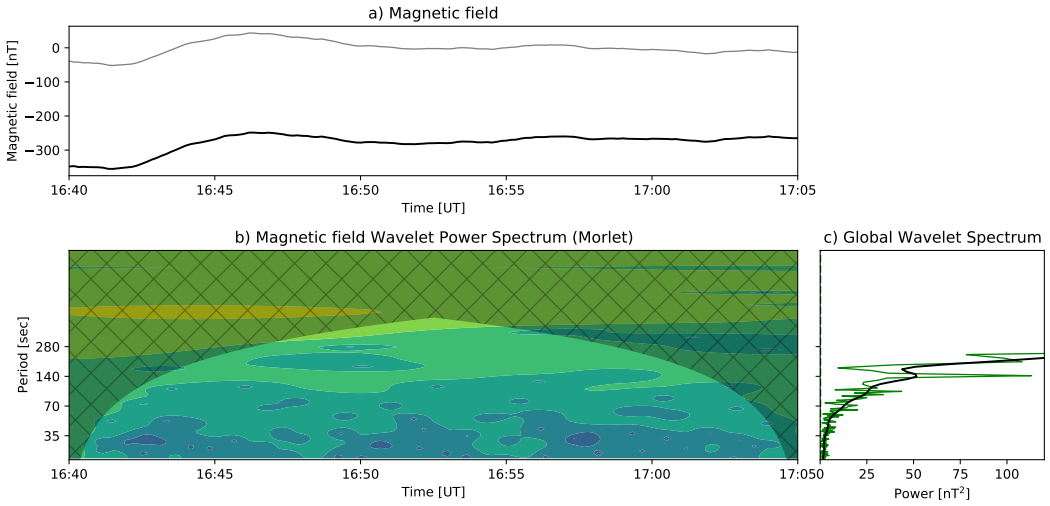

317 **Figure 9.** Wavelet transform analysis of the geomagnetic field oscillations at Arctic Village,
318 Alaska (ARC) for the E-component, nT, between 16:40 and 17:05 UT: (a) original (black) series
319 and inverse (gray) wavelet transform; (b) the normalized wavelet power spectrum and shaded
320 cone of influence and (c) the global wavelet (black) and Fourier power spectra (green). Note that
321 period scale is logarithmic.

322 4 Modeling of magnetospheric observations

323 The Lyon-Fedder-Mobarry (LFM) global magnetosphere model, as hosted by the
324 NASA Community Coordinated Modeling Center (CCMC), was used to further inves-
325 tigate the magnetopause configuration in the vicinity of the Cluster spacecraft during
326 the event time frame. The LFM model solves the ideal magnetohydrodynamic (MHD)
327 equations to simulate the 3D interaction between the solar wind and the Earth's mag-
328 netosphere. Further description of the simulation code and its numerical methods can
329 be found in *Lyon et al.* [2004] and *Merkin and Lyon* [2010]. The LFM model can effec-
330 tively resolve the KHI due to its low diffusion numerical scheme and has been used in
331 previous studies of the KHI [*Merkin et al.*, 2013; *Sorathia et al.*, 2019].

332 The simulation was driven by measured solar wind parameters provided by the vir-
333 tual OMNI database [*King and Papitashvili*, 2005] including plasma density, velocities,
334 IMF vector, and dipole tilt angle. The simulation was run from 16:00 to 17:30 UT and
335 snapshots of its development at 16:37 and 16:41 UT are shown in Figure 10. The back-
336 ground color represents plasma density and the arrows show the velocity vectors. The
337 triangles show the actual location of the four Cluster spacecraft during the event. From

the figure, it can be seen that the lower density magnetosphere (dark blue) has developed rolled-up waves at the border with the higher density magnetosheath (light blue). At 16:37 the KH waves are not clearly visible on the dusk-side (see supplemental materials for full dawn/dusk snapshot). This is because the horizontal component of the IMF for this event is in the Parker Spiral orientation, making the dusk flank downstream of the quasi-perpendicular bow shock, where the stronger magnetic tension can stabilize the KHI, which is consistent with previous simulation studies of the KHI during Parker Spiral IMF [*Nykyri*, 2013] and observations from 6 years of THEMIS data [*Henry et al.*, 2017].

Figure 11 displays the simulation driven for constant solar wind and IMF conditions but without any solar wind dynamic pressure variations in order to check whether the ULF waves were caused by pressure driven surface waves or by KHI driven waves. Because the waves were formed in the simulation without any solar wind fluctuations, the non-linear waves seen by Cluster were most likely generated by the KHI. Note that for the unstable boundary conditions, the KHI can be seeded by any perturbation such as magnetic fluctuations [*Ma et al.*, 2014b], velocity fluctuations [*Nykyri et al.*, 2017], pressure fluctuations, or any combination of these. The magnitude and frequency of the perturbation can affect the non-linear stage of the instability [*Nykyri et al.*, 2017]. Based on the present simulation, the source region for the KHI appears to be on the dayside magnetopause where the magnetosheath flow first diverges dawnward. Note that this is a cut at Z =-9.4 R_E and low latitude reconnection is also likely to operate which can act as a seed perturbation for the KHI [*Ma et al.*, 2014b].

All the simulation results and more details on the settings of both runs can be found at $https://ccmc.gsfc.nasa.gov/$ with run-name $Katariina\_Nykyri\_111218\_1$ (real solar wind and IMF based run) and $Katariina\_Nykyri\_070119\_8$ (synthetic run without solar wind dynamic pressure variations). A movie of the simulation can be found in the supplementary materials. More detailed high-resolution 3D MHD simulations with test particles and Cluster data comparison is left for our future work.

5 Discussion

The time frame of study showed periodical observations of magnetospheric and magnetosheath plasma populations which can be interpreted as the KHI:

(1) Persistent bipolar B_N fluctuations occurred such that the B_N=0 crossings were not observed simultaneously with the total pressure maxima. Rather, the magnetic field magnitude and normal component maxima were aligned with the pressure maxima, indicating that the spacecraft were traversing the rolled-up Kelvin-Helmholtz waves [*Hasegawa et al.*, 2004; *Hasegawa*, 2012]. This differs from instances of observing either FTEs or persistent surface waves. In the case of FTE observation, the pressure maxima is expected at its core and the bipolar B_N fluctuations are separated by quiet periods with repetition period longer than four minutes [*Kavosi and Raeder*, 2015]. In the case of persistent surface waves, the pressure maxima will be associated with the bipolar B_N=0 crossings. These KHW magnetic field and total pressure signatures occurred in conjunction with periodical observations of magnetospheric and magnetosheath plasma populations, indicating that the KHI had developed into the vortices necessary for energy transport across the magnetopause [*Moore et al.*, 2016];

(2) The plasma conditions of instability growth for KHW at the magnetopause were satisfied;

(3) The rolled-up vortices were also clearly seen in LFM simulation results for the event, confirming that the solar wind conditions were favorable for KHW development;

(4) The fastest growing Kelvin-Helmholtz wavelength, λ, and frequency, f, depend on the boundary layer thickness, Δ, such that:

$$\lambda = (2 \ldots 4)\Delta\pi \tag{4}$$

so the fastest growing frequency can be calculated from:

$$f = v_{phase}/((2 \ldots 4)\Delta\pi) \tag{5}$$

(See *Miura and Pritchett* [1982]).

Using the spatial and temporal development of the KHWs seen in Figure 10, the phase velocity between 16:37 and 16:41 UT can be estimated to be $v_{phase} \approx 3.5$ R_E/240 s $\approx$ 93 km/s. Assuming the shear layer thickness, Δ, to be 1500 km and calculating for the frequency using the above equation gives $f \approx$ 4.9-9.8 mHz, which is within the Pc5/Pc4

range. This is in agreement with the Cluster-observed magnetopause KHW associated with reconnection frequency peak of about 7 mHz (140 s);

(5) The analysis of the magnetopause shear angle confirmed the configuration to be favorable for the KHI. The event was recorded at $X_{GSM} \approx$ -10 R_E, $Y_{GSM} \approx$ -16 R_E, $Z_{GSM} \approx$ -8 R_E, putting it in the blue zone of Figure 8.

However, most of the KHI vortices observed in this event were followed by reconnection events as indicated by the Walén relation, the presence of deHoffman-Teller frames and field-aligned ion beams. For the southward IMF orientation, both magnetic reconnection and KHI can be observed at the same time [*Ma et al.*, 2014a,b]. Such coupling is well-illustrated in modeling by *Ma et al.* [2014a] in Figure 11 at t= 124 s. This event demonstrates the complexity of the instabilities generated at the magnetopause.

It has been shown that when the IMF has a strong Parker spiral component, the KHI can develop with tilted k-vectors with respect to the shear flow plane to maximize the onset condition [*Adamson et al.*, 2016; *Henry et al.*, 2017; *Nykyri et al.*, 2006], which could explain why KHWs were observed by Cluster at high latitudes. Source regions for longer wavelengths and lower frequencies are expected further down the magnetotail. For the present KHI associated with reconnection event, there are three possible source regions: one close to the subsolar point where magnetosheath flow first starts to diverge and where KHI growth may be enhanced both by the solar wind velocity and pressure fluctuations [*Nykyri et al.*, 2017] and dayside reconnection [*Ma et al.*, 2014b]; one at the high-latitude southern dawn sector of the cusp; and one farther down the tail, where the flow from tail reconnection is moving earthward and forms a shear layer farther along the tail. This velocity shear layer is observable in the LFM simulation plot. Most relevant for the present event are the first two, and future work will need to address the possible KHI associated with reconnection interference from multiple sources.

ULF waves in the magnetosphere have been correlated with changing or high-speed solar wind conditions. For one, dynamic pressure variations are known to generate pulsations [*Hwang and Sibeck*, 2016]. However, the solar wind speed, IMF magnitude, Alfvénic Mach number (not shown), and flow pressure all remained nearly constant during the event, ruling out the likelihood of the ULF waves being driven directly by pressure perturbations. There were solar wind pressure pulsations preceding the event which may have acted as seed perturbations at the subsolar point, providing for the propagation and

development of the event KHWs seen further down the flank [*Hartinger et al.*, 2015]. In fact, three of the THEMIS spacecraft situated at the subsolar point during this event recorded signatures of significant boundary motion, including pressure perturbations, which further supports this hypothesis. Figure 12 shows the pressure tensor for the $xx-$, $yy-$, and $zz-$components (red, blue, green, respectively) recorded by the Electrostatic Analyzer (ESA) onboard THEMIS-E (P4). The ion pressure moment data were obtained from reduced-mode data, which has a degraded angular resolution, but high time resolution ($\sim$ 3 s). Similar plots for THEMIS-C and THEMIS-D can be found in the supplementary materials.

6 Conclusions

The current debate surrounding the extent of magnetospheric effects caused by Kelvin-Helmholtz waves at the magnetopause remains an exciting topic as more and more in situ observations become available for analysis. This process' role in the generation of ULF waves at the Earth's ground, in particular, continues to be uncertain since so many potential drivers have been identified. The event scrutinized in this article will hopefully aid in confirming the KHI associated with reconnection as one of the direct ULF-driving mechanisms.

On 3 July 2007 Cluster encountered KHWs at the magnetopause. Signatures of these waves included bipolar fluctuations in the magnetic field normal component at the edge of total pressure maxima and alternations of the low-density, low-speed, and high-energy magnetospheric plasma with the high-density, high-speed, and low energy magnetosheath plasma. The plasma conditions for KHI grow at the magnetopause were satisfied. The KHWs exhibited frequency peaks in the Pc4 range which is typical for this instability. LFM simulations of the observed event conditions also resulted in KHWs at the magnetopause. Most of the observed KHI vortices were followed by reconnection as indicated by the Walén relation, the presence of deHoffman-Teller frames and field-aligned ion beams.

During the same time as the event at the magnetopause, there were Pc4 ULF perturbations recorded at ground-based geomagnetic stations. These pulsations were observed around the location of the foot point corresponding to the field line of the location of the spacecraft recordings. Solar wind conditions during the event were rather steady.

The solar wind speed was low and the IMF magnitude was nearly constant. Only minimal pressure perturbations were recorded and the B_Z component of the IMF remained southward without strong fluctuations.

The conditions recorded during this case study provide evidence for the likelihood that Pc4 ULF waves can be generated by the KHI associated with reconnection at the magnetopause. It is probable that other KHI-ULF events with similar solar wind conditions exist, but further study is needed before the ubiquity of such an event can be declared. However, the fact that this event directly links the KHI associated with reconnection to ULF perturbations at the ground solidifies the conclusion that the KHI plays a powerful role in the transfer of energy from the solar wind to the magnetosphere.

Acknowledgments

The authors would like to thank the Cluster Science Archive (https://csa.esac.esa.int) team for providing the data and assistance in obtaining the CIS plot. We gratefully acknowledge the SuperMAG collaborators (http://supermag.jhuapl.edu/info/?page=acknowledgement). We also acknowledge use of NASA/GSFC's Space Physics Data Facility's OMNIWeb (or CDAWeb or ftp - see https://cdaweb.sci.gsfc.nasa.gov/index.html) service, and OMNI data (https://omniweb.gsfc.nasa.gov). We acknowledge NASA contract NAS5-02099 and V. Angelopoulos for use of data from the THEMIS Mission (http://themis.igpp.ucla.edu/index.shtml); specifically, C. W. Carlson and J. P. McFadden for use of ESA data. The results presented in this paper rely on the data collected at the Arctic Village and Kaktovik magnetometers, provided by the Geophysical Institute Magnetometer Array operated by the Geophysical Institute, University of Alaska (https://www.gi.alaska.edu/monitors/magnetometer/archive).

Global LFM MHD simulations have been provided by the Community Coordinated Modeling Center at Goddard Space Flight Center through their public runs on request system (http://ccmc.gsfc.nasa.gov).

The work of J. Gorman, E. E. Grigorenko, L. V. Kozak, and E. A. Kronberg is supported by the Volkswagen Foundation under grant Az 90 312. Work by K. Nykyri is supported by the NASA grant ##NNX17AI50G. The work of E. A. Kronberg is also supported by German Research Foundation (DFG) under number KR 4375/2-1 within SPP "Dynamic Earth".

References

Adamson, E., K. Nykyri, and A. Otto (2016), The Kelvin-Helmholtz instability under Parker-spiral interplanetary magnetic field conditions at the magnetospheric flanks, *Advances in Space Research*, *58*, 218–230, doi:https://doi.org/10.1016/j.asr.2015.09.013.

Agapitov, O., K.-H. Glassmeier, F. Plaschke, H.-U. Auster, D. Constantinescu, V. Angelopoulos, et al. (2009), Surface waves and field line resonances: A THEMIS case study, *Journal of Geophysical Research*, *114*(A00C27), doi:https://doi.org/10.1029/2008JA013553.

Balogh, A., et al. (2001), The Cluster magnetic field investigation: Overview of in-flight performance and initial results, *Annales Geophysicae*, *19*, 1207–1217.

Bentley, S. N., C. E. J. Watt, M. J. Owens, and I. J. Rae (2018), ULF wave activity in the magnetosphere: Resolving solar wind interdependencies to identify driving mechanisms, *Journal of Geophysical Research: Space Physics*, *123*, 2745–2771, doi:https://doi.org/10.1002/2017JA024740.

Boscher, D., S. Bourdarie, P. O'Brien, and T. Guild (2012), Irbem-lib library.

Dimmock, A. P., and K. Nykyri (2013), The statistical mapping of magnetosheath plasma properties based on THEMIS measurements in the magnetosheath interplanetary medium reference frame, *Journal of Geophysical Research: Space Physics*, *118*, 4963–4976, doi:https://doi.org/10.1002/jgra.50465.

Dougal, E. R., K. Nykyri, and T. W. Moore (2013), Mapping of the quasi-periodic oscillations at the flank magnetopause into the ionosphere, *Annales Geophysicae*, *31*, 1993–2011, doi:https://doi.org/10.5194/angeo-31-1993-2013.

Dunlop, M. W., J.-Y. Yang, Y.-Y. Yang, C. Xiong, H. Lühr, Y. V. Bogdanova, et al. (2015), Simultaneous field-aligned currents at Swarm and Cluster satellites, *Geophysical Research Letters*, *42*, 3683–3691, doi:https://doi.org/10.1002/2015GL063738.

Elkington, S. R., M. K. Hudson, and A. A. Chan (2003), Resonant acceleration and diffusion of outer zone electrons in an asymmetric geomagnetic field, *Journal of Geophysical Research*, *108*(A3), doi:https://doi.org/10.1029/2001JA009202.

Escoubet, C. P., R. Schmidt, and M. L. Goldstein (1997), Cluster—Science and mission overview, *Space Science Reviews*, *79*, 11–32.

Fairfield, D. H., A. Otto, T. Mukai, S. Kokubun, R. P. Lepping, J. T. Steinberg, A. J. Lazarus, and T. Yamamoto (2000), Geotail observations of the Kelvin-Helmholtz instability at the eqatorial magnetotail boundary for parallel northward fields, *J. Geophys. Res.*, *105*, 21,159–21,174.

Gjerloev, J. W. (2012), The SuperMAG data processing technique, *Journal of Geophysical Research*, *117*(A09213), doi:https://doi.org/10.1029/2012JA017683.

Hartinger, M. D., F. Plaschke, M. O. Archer, D. T. Welling, M. B. Moldwin, and A. Ridley (2015), The global structure and time evolution of dayside magnetopause surface eigenmodes, *Geophysical Research Letters*, *42*, 2594–2602, doi:https://doi.org/10.1002/2015GL063623.

Hasegawa, A., and L. Chen (1974), Theory of magnetic pulsations, *Space Science Reviews*, *16*, 347–359.

Hasegawa, H. (2012), Structure and dynamics of the magnetopause and its boundary layers, *Monographs on Environment, Earth and Planets*, *1*(2), 71–119, doi:https://doi.org/10.5047/meep.2012.00102.0071.

Hasegawa, H., M. Fujimoto, T.-D. Phan, H. Rème, A. Balogh, M. W. Dunlop, et al. (2004), Transport of solar wind into Earth's magnetosphere through rolled-up Kelvin-Helmholtz vortices, *Nature*, *430*, 755–758, doi:https://doi.org/10.1038/nature02799.

Henry, Z. W., K. Nykyri, T. W. Moore, A. P. Dimmock, and X. Ma (2017), On the dawn-dusk asymmetry of the Kelvin-Helmholtz instability between 2007 and 2013, *Journal of Geophysical Research: Space Physics*, *122*(12), 11,888–11,900, doi:https://doi.org/10.1002/2017JA024548.

Hwang, K.-J., and D. G. Sibeck (2016), *Role of low-frequency boundary waves in the dynamics of the dayside magnetopause and the inner magnetosphere*, chap. 13, pp. 213–239, Hoboken, NJ: John Wiley, doi:https://doi.org/10.1002/9781119055006.ch13.

Johnson, J. R., S. Wing, and P. A. Delamere (2014), Kelvin Helmholtz Instability in Planetary Magnetospheres, *Space Science Reviews*, *184*(1-4), 1–31, doi:10.1007/s11214-014-0085-z.

Kavosi, S., and J. Raeder (2015), Ubiquity of Kelvin-Helmholtz waves at Earth's magnetopause, *Nature Communications*, *6*(7019), doi:https://doi.org/10.1038/ncomms8019.

Khrabrov, A. V., and B. U. O. Sonnerup (1998), Orientation and motion of current layers: Minimization of the Faraday residue, *Geophysical Research Letters*, *25*(13), 2373–2376.

King, J. H., and N. E. Papitashvili (2005), Solar wind spatial scales in and comparisons of hourly Wind and ACE plasma and magnetic field data, *Journal of Geophysical Research*, *110*(A02104), doi:https://doi.org/10.1029/2004JA010649.

Kronberg, E. A., E. E. Grigorenko, D. L. Turner, P. W. Daly, Y. Khotyaintsev, and L. Kozak (2017), Comparing and contrasting dispersionless injections at geosynchronous orbit during a substorm event, *Journal of Geophysical Research: Space Physics*, *122*, 3055–3072, doi:https://doi.org/10.1002/2016JA023551.

Laakso, H., C. Perry, S. McCaffrey, D. Herment, A. J. Allen, C. C. Harvey, et al. (2010), *Cluster Active Archive: Overview*, pp. 3–37, Springer.

Lotko, W., A. V. Streltsov, and C. W. Carlson (1998), Discrete auroral arc, electrostatic shock and suprathermal electrons powered by dispersive, anomalously resistive field line resonance, *Geophysical Research Letters*, *25*(24), 4449–4452.

Lyon, J. G., J. A. Fedder, and C. M. Mobarry (2004), The Lyon-Fedder-Mobarry (LFM) global MHD magnetospheric simulation code, *Journal of Atmospheric and Solar-Terrestrial Physics*, *66*(1333).

Ma, X., A. Otto, and P. A. Delamere (2014a), Interaction of magnetic reconnection and Kelvin-Helmholtz modes for large magnetic shear: 1. Kelvin-Helmholtz trigger, *Journal of Geophysical Research: Space Physics*, *119*, 781–797, doi:https://doi.org/10.1002/2013JA019224.

Ma, X., A. Otto, and P. A. Delamere (2014b), Interaction of magnetic reconnection and Kelvin-Helmholtz modes for large magnetic shear: 2. Reconnection trigger, *Journal of Geophysical Research: Space Physics*, *119*, 808–820, doi:https://doi.org/10.1002/2013JA019225.

Merkin, V. G., and J. G. Lyon (2010), Effects of the low-latitude ionospheric boundary condition on the global magnetosphere, *Journal of Geophysical Research*, *115*(A10202), doi:https://doi.org/10.1029/2010JA015461.

Merkin, V. G., J. G. Lyon, and S. G. Claudepierre (2013), Kelvin-Helmholtz instability of the magnetospheric boundary in a three-dimensional global MHD simulation during northward IMF conditions, *Journal of Geophysical Research: Space Physics*, *118*, 5478–5496, doi:https://doi.org/10.1002/jgra.50520.

Miura, A., and P. L. Pritchett (1982), Nonlocal stability analysis of the MHD Kelvin-Helmholtz instability in a compressible plasma, *Journal of Geophysical Research*, *87*, 7431–7444, doi:https://doi.org/10.1029/JA087iA09p07431.

Moore, T. W., K. Nykyri, and A. P. Dimmock (2016), Cross-scale energy transport in space plasmas, *Nature Physics*, *12*, 1164–1169, doi:https://doi.org/10.1038/NPHYS3869.

Moore, T. W., K. Nykyri, and A. P. Dimmock (2017), Ion-scale wave properties and enhanced ion heating across the low-latitude boundary layer during Kelvin-Helmholtz instability, *Journal of Geophysical Research: Space Physics*, *122*, 11,128—-11,153, doi:https://doi.org/10.1002/2017JA024591.

Nykyri, K. (2013), Impact of MHD shock physics on magnetosheath asymmetry and Kelvin-Helmholtz instability, *Journal of Geophysical Research: Space Physics*, *118*, 5068—-5081, doi:https://doi.org/10.1002/jgra.50499.

Nykyri, K., and A. P. Dimmock (2016), Statistical study of the ULF Pc4-Pc5 range fluctuations in the vicinity of earth's magnetopause and correlation with the low latitude boundary layer thickness, *Advances in Space Research*, *58*, 257–267, doi:https://doi.org/10.1016/j.asr.2015.12.046.

Nykyri, K., and A. Otto (2001), Plasma transport at the magnetospheric boundary due to reconnection in Kelvin-Helmholtz vortices, *Geophysical Research Letters*, *28*(18), 3565–3568.

Nykyri, K., A. Otto, B. Lavraud, C. Mouikis, L. Kistler, A. Balogh, and H. Rème (2006), Cluster observations of reconnection due to the Kelvin-Helmholtz instability at the dawn side magnetospheric flank, *Annales Geophysicae*, *24*, 2619–2643.

Nykyri, K., X. Ma, A. Dimmock, C. Foullon, A. Otto, and A. Osmane (2017), Influence of velocity fluctuations on the Kelvin-Helmholtz instability and its associated mass transport, *Journal of Geophysical Research: Space Physics*, *122*, 9489—-9512, doi:https://doi.org/10.1002/2017JA024374.

Otto, A., and D. H. Fairfield (2000), Kelvin-Helmholtz instability at the magnetotail boundary: MHD simulation and comparison with Geotail observations, *J. Geophys. Res.*, *105*, 21,175–21,190.

Paschmann, G., S. Haaland, B. U. Ö. Sonnerup, H. Hasegawa, E. Georgescu, B. Klecker, T. D. Phan, H. Rème, and A. Vaivads (2005), Characteristics of the near-tail dawn magnetopause and boundary layer, *Annales Geophysicae*, *23*(4),

1481–1497, doi:10.5194/angeo-23-1481-2005.

Rae, I. J., E. F. Donovan, I. R. Mann, F. R. Fenrich, C. E. J. Watt, D. K. Milling, et al. (2005), Evolution and characteristics of global Pc5 ULF waves during a high solar wind speed interval, *Journal of Geophysical Research*, *110*(A12211), doi:https://doi.org/10.1029/2005JA011007.

Rème, H., et al. (2001), First multispacecraft ion measurements in and near the Earth' s magnetosphere with the identical Cluster ion spectrometry (CIS) experiment, *Annales Geophysicae*, *19*, 1303–1354.

Shumko, M., J. Sample, A. Johnson, J. B. Blake, A. B. Crew, H. E. Spence, et al. (2018), Microburst scale size derived from multiple bounces of a microburst simultaneously observed with the FIREBIRD-II CubeSats, *Geophysical Research Letters*, *45*, 8811–8818, doi:https://doi.org/10.1029/2018GL078925.

Sonnerup, B. U. Ö., G. Paschmann, and T. D. Phan (1995), Fluid Aspects of Reconnection at the Magnetopause: In Situ Observations, *Washington DC American Geophysical Union Geophysical Monograph Series*, *90*, 167, doi:10.1029/GM090p0167.

Sorathia, K., V. G. Merkin, A. Y. Ukhorskiy, R. C. Allen, K. Nykyri, and S. Wing (2019), Solar wind ion entry into the magnetosphere during northward IMF, *Journal of Geophysical Research: Space Physics*, *124*, 5461—-5481, doi:https://doi.org/10.1029/2019JA026728.

Southwood, D. J. (1974), Some features of field line resonances in the magnetosphere, *Planetary and Space Science*, *22*, 483–491.

Trattner, K. J., J. S. Mulcock, S. M. Petrinec, and S. A. Fuselier (2007), Probing the boundary between anti-parallel and component reconnection during southwards interplanetary magnetic field conditions, *Journal of Geophysical Research*, *112*(A08210), doi:https://doi:10.1029/2007JA012270.

Trattner, K. J., J. L. Burch, R. Ergun, S. Eriksson, S. A. Fuselier, B. L. Giles, et al. (2017), The MMS dayside magnetic reconnection locations during Phase 1 and their relation to the predictions of the Maximum Magnetic Shear model, *Journal of Geophysical Research: Space Physics*, *122*, 11,991–12,005, doi:https://doi.org/10.1002/2017JA024488.

Walker, A. D. M. (1981), The Kelvin-Helmholtz instability in the low-latitude boundary layer, *Planetary and Space Science*, *829*, 1119–1133.

Wang, C.-P., R. Thorne, T. Z. Liu, M. D. Hartinger, T. Nagai, V. Angelopoulos, et al. (2017), A multispacecraft event study of Pc5 ultralow-frequency waves in the magnetosphere and their external drivers, *Journal of Geophysical Research: Space Physics*, *122*, 5132–5147, doi:https://doi.org/10.1002/2016JA023610.

Wing, S., J. R. Johnson, P. T. Newell, and C.-I. Meng (2005), Dawn-dusk asymmetries, ion spectra, and sources in the northward interplanetary magnetic field plasma sheet, *Journal of Geophysical Research*, *110*(A08205), doi: https://doi.org/10.1029/2005JA011086.

Yu, Y., and A. J. Ridley (2013), Exploring the influence of ionospheric O+ outflow on magnetospheric dynamics: The effect of outflow intensity, *Journal of Geophysical Research: Space Physics*, *118*, 5522–5531, doi:https://doi.org/10.1002/jgra.50528.

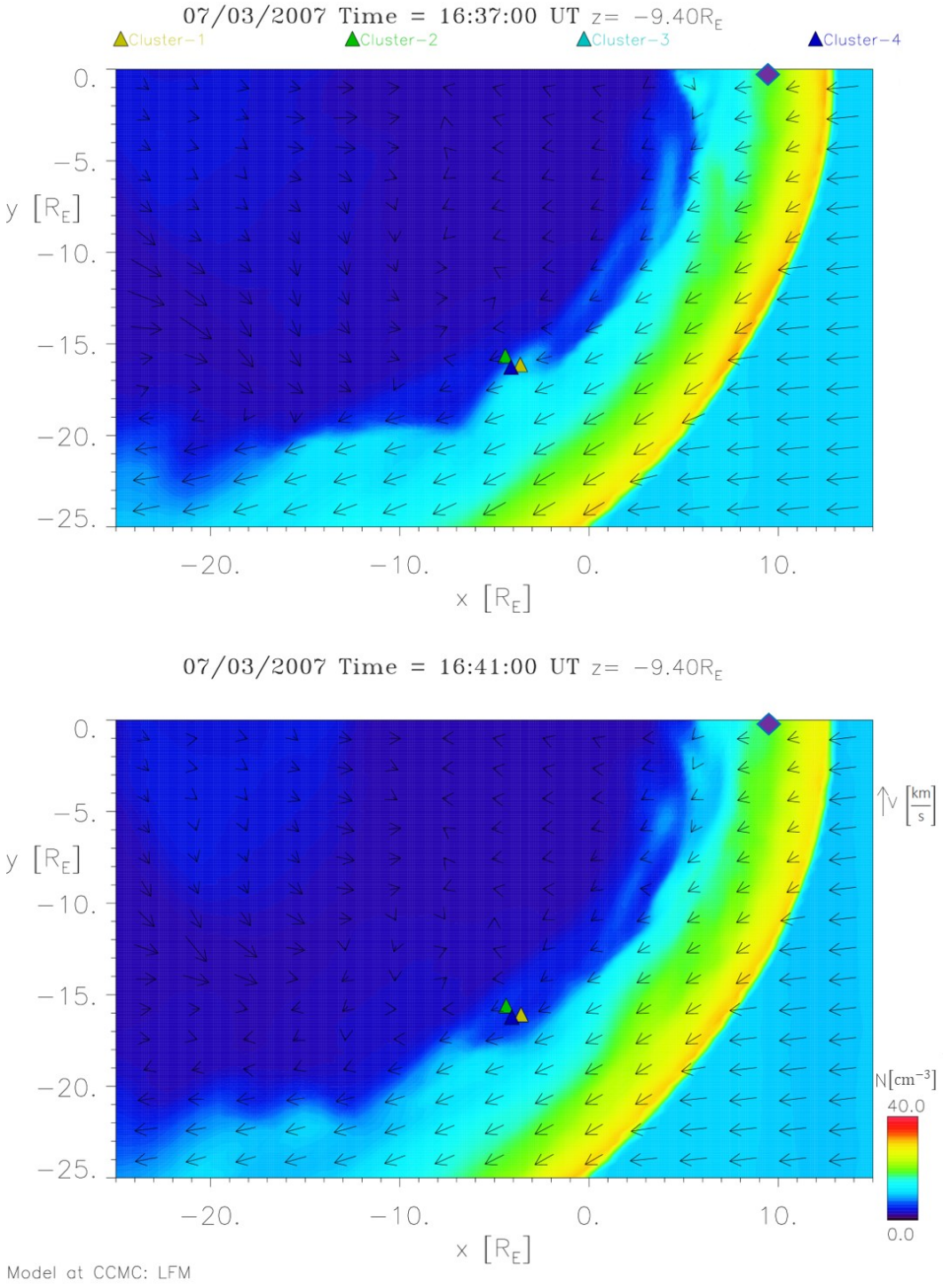

Figure 10. Snapshot of the Global MHD (LFM-model) simulation, driven with solar wind dynamic pressure variations, in the X, Y -plane with Z = -9.4 R_E (solar magnetic coordinates) for 3 July 2007 at 16:37 (top) and 16:41 UT (bottom). Colors represent plasma density (see color bar), arrows represent plasma velocity, and the triangles show the location of the four Cluster spacecraft. The purple diamond denotes the approximate (x, y) location of the THEMIS spacecraft (with $Z_{GSE} \approx$ -2.4 R_E).

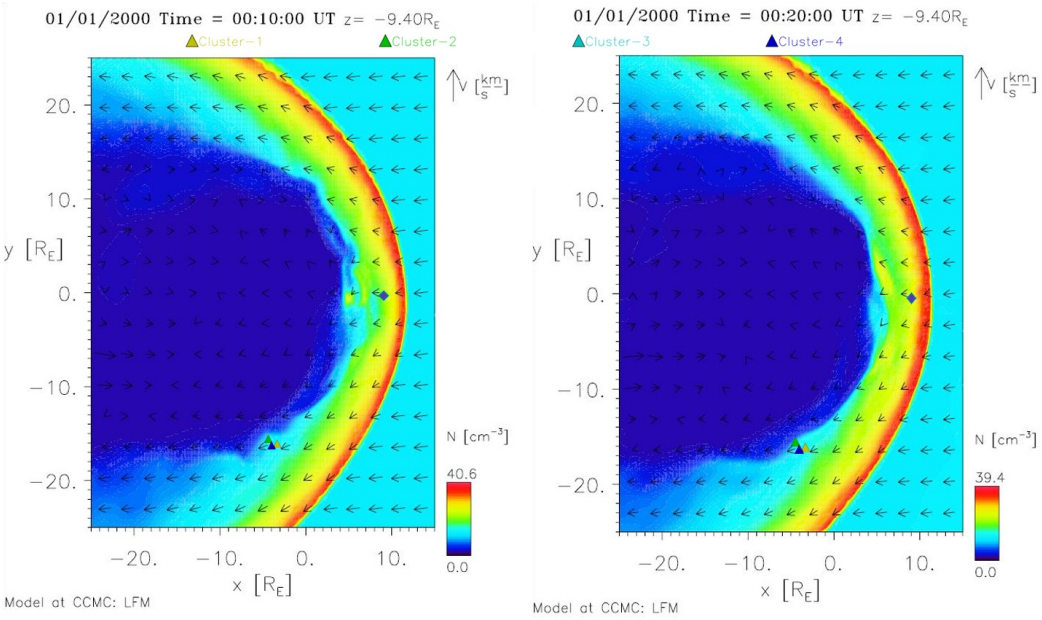

Figure 11. Snapshot of the Global MHD (LFM-model) simulation, driven with constant IMF orientation and without solar wind dynamic pressure variations, in the X, Y -plane with Z = -9.4 R_E (solar magnetic coordinates) for conditions characteristic of 3 July 2007 between 16:00 and 17:30 UT. The upper figure show a snapshot taken at 10 minutes into the simulation, and the lower figure shows a snapshot taken at 20 minutes. Colors represent plasma density (see color bar), arrows represent plasma velocity, and the triangles show the location of the four Cluster spacecraft. The purple diamond denotes the approximate (x, y) location of the THEMIS spacecraft (with $Z_{GSE} \approx$ -2.4 R_E).

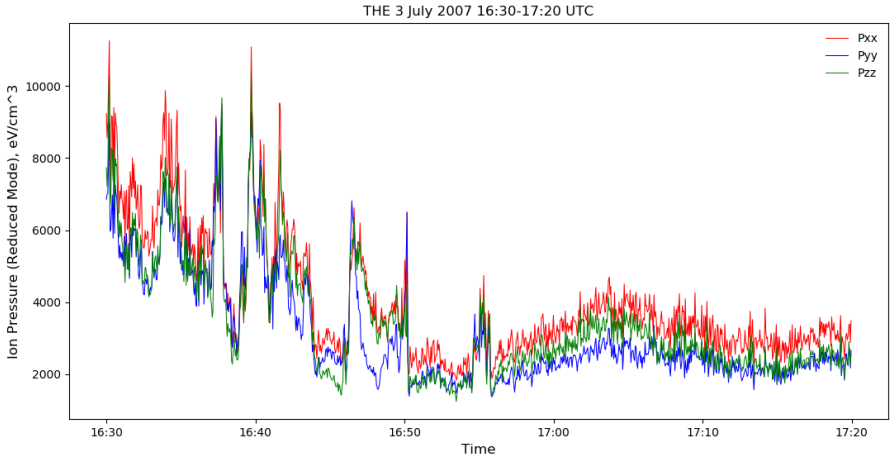

Figure 12. THEMIS-E pressure tensor for the $xx-$ (red), $yy-$ (blue), and $zz-$components (green), eV/cm^3, recorded by the Electrostatic Analyzer (ESA). Reduced mode data are shown for 3 July 2007 from 16:30-17:20 UT.